

## Journal Pre-proof

Three-dimensional bioprinted cancer models: a powerful platform for investigating tunneling nanotube-like cell structures in complex microenvironments

Helena Herrada-Manchón, Lucía Celada, David Rodríguez-González, M. Alejandro Fernández, Enrique Aguilar, María-Dolores Chiara



PII: S0928-4931(21)00497-5

DOI: <https://doi.org/10.1016/j.msec.2021.112357>

Reference: MSC 112357

To appear in: *Materials Science & Engineering C*

Received date: 1 May 2021

Revised date: 10 July 2021

Accepted date: 2 August 2021

Please cite this article as: H. Herrada-Manchón, L. Celada, D. Rodríguez-González, et al., Three-dimensional bioprinted cancer models: a powerful platform for investigating tunneling nanotube-like cell structures in complex microenvironments, *Materials Science & Engineering C* (2021), <https://doi.org/10.1016/j.msec.2021.112357>

This is a PDF file of an article that has undergone enhancements after acceptance, such as the addition of a cover page and metadata, and formatting for readability, but it is not yet the definitive version of record. This version will undergo additional copyediting, typesetting and review before it is published in its final form, but we are providing this version to give early visibility of the article. Please note that, during the production process, errors may be discovered which could affect the content, and all legal disclaimers that apply to the journal pertain.

# Three-dimensional bioprinted cancer models: a powerful platform for investigating tunneling nanotube-like cell structures in complex microenvironments

**Helena Herrada-Manchón<sup>1,2,6</sup>, Lucía Celada<sup>3,4,6</sup>, David Rodríguez-González<sup>1,2</sup>, M. Alejandro Fernández<sup>2,7</sup>, Enrique Aguilar<sup>1</sup>, and María-Dolores Chiara<sup>3,4,5,7</sup>**

<sup>1</sup> Centro de Innovación en Química Avanzada (ORFEO-CINQA), Instituto Universitario de Química Organometálica “Enrique Moles”, Departamento de Química Orgánica e Inorgánica, Universidad de Oviedo, 33006, Spain

<sup>2</sup> Fundación Idonial, Parque Científico y Tecnológico de Gijón, 26205, Gijón, Spain

<sup>3</sup> Instituto de Investigación Sanitaria del Principado de Asturias, 33011, Oviedo, Spain

<sup>4</sup> CIBERONC, 28029, Madrid, Spain

<sup>5</sup> Instituto Universitario de Oncología del Principado de Asturias, Universidad de Oviedo, 33006, Oviedo, Spain

<sup>6</sup> Equal contribution

<sup>7</sup> Authors to whom any correspondence should be addressed.

*Corresponding author:*

María Dolores Chiara

Instituto de Investigación Sanitaria del Principado de Asturias

Av de Roma s/n

33011-Oviedo

Spain

E-mail: mdchiara.uo@uniovi.es

**Abstract**

Bioprinting technology offers layer-by-layer positioning of cells within 3D space with complexity and a defined architecture. Cancer models based in this biofabrication technique are important tools to achieve representative and realistic *in vivo* conditions of the tumor microenvironment. Here, we show the development of a proof-of-concept three-dimensional bioprinted cancer model that successfully recapitulates the intercellular communication via the assembly of functional tunneling nanotube (TNT)-like cell projections. Different combinations of collagen-containing culture medium, sodium alginate and gelatin were initially prepared and rheologically evaluated. The optimized mixture was used to print two preliminary 3D models for cancer cell seeding. Favourable results in cell viability and proliferation led to the inclusion of 786-O renal cancer cells into the biomaterial mixture to directly bioprint the most suitable 3D model with embedded cells. Bioprinted cells remained viable for at least 15 days of culture and proliferated. More importantly, these cancer cells were able to build TNT-like cellular projections inside the hydrogel that established direct contacts between distant cells. We show that these structures were used as channels for the scrolling and intercellular transfer of mitochondria thus reproducing TNT's function in 2D culture systems. This 3D bioprinted renal cancer model provides a novel alternative tool for studying the functional relevance of TNT-like structures in tumorigenesis and anticancer drug susceptibility in a highly controlled and reproducible tumor microenvironment.

**Keywords:** 3D bioprinting, cancer models, cell-to-cell communication, tunneling nanotubes

## 1. Introduction

Cell culture is an extensively used tool for the *in vitro* study of cell biology, tissue morphology, or disease mechanisms. Specifically, two-dimensional (2D) cell culture models have played an important role in enhancing our understanding of cancer development and progression. However, it is well-recognized that those systems fail to accurately represent the tumor ecosystems or recapitulate in a precise manner the cellular interactions that take place in the complex cancer tissues [1,2].

Cells growing in monolayers have an unlimited access to the medium ingredients (oxygen, metabolites, growth factors...), which becomes an inconvenient when trying to mimic real cancer tissues where nutrient availability is highly heterogeneous due to the intrinsic complexity of the tumor tissue architecture [2–4]. Furthermore, the bidirectional flow of information between the cellular and extracellular components of the tumor ecosystem cannot be recapitulated in the non-physiological 2D cell culture models [5,6]. On another hand, there are cell processes observed in 2D culture models that do not have a correlate *in vivo* [7]. This is particularly relevant in the case of the novel and revolutionary field of cell-to-cell communication through the tunneling nanotube (TNT)-like projections. TNTs are thin membrane tubes that connect distant cells and function as channels for the intercellular transport of diverse cargo including cellular organelles such as mitochondria [8]. TNTs were initially identified in 2D cancer cell culture models what raised the question whether their formation could be a consequence of the artificial conditions of the cell culture [9]. TNTs' heterogeneity, lability and poor structural characterization is still hampering unequivocal demonstration of their presence in complex cancer tissues or even 3D culture conditions thus raising skepticism in the scientific community about their existence and their putative pathological role in cancer [10].

The analysis of TNTs in living animals would provide a wealth of information about cancer cell behavior in a physiopathologically relevant context. However, *in vivo* models are too complex to study TNT-mediated specific interactions between cells [1,2]. Consequently, 3D cell cultures is a working alternative and, particularly, 3D bioprinting is showing promise for the development of *in vitro* models in a different approach [11–13].

Bioprinting technology offers layer-by-layer positioning of cells within 3D space, with the shape and architecture defined using computer-aided design (CAD) [14,15]. Broadly categorized as either extrusion, droplet, or laser-based bioprinting, provides an automatized, precise and repeatable method particularly useful to mimic tumor microenvironment [16–19]. The use of 3D bioprinted tumors is increasing in areas like tumor biology, migration, invasion, and metastasis, as well as in high-throughput drug screening and validation, even providing the possibility for personalized medicine [20–23].

It is important to highlight that replicating 3D cell-systems is extremely challenging and cannot be achieved without a strong work in bioink formulation and rheological analysis. The combination of biomaterials, cells and other key factors to form a printable hydrogel, plays a fundamental role in subsequently obtaining a structure with high shape fidelity, in addition to enough cell viability [15,24].

In this work, syringe-based extrusion bioprinting encompassed, firstly, the fabrication of preliminary 3D-matrices to test viability, adhesion and cell growth. After this first approach, and the selection of the most suitable 3D model, a cell-loaded formulation was directly deposited generating multilayer grid structures to represent tumor models for studying cancer cell behavior. We show here that this single-cell model is useful as proof-of-concept model that confirm not only the possibility of bioprinting cancer cells, but also the observation of direct cell-to-cell communication and mitochondria trafficking via TNT-like protrusions which, to the best of our knowledge, has not been described before in this setting and for a renal cancer cell line. The discovery of TNT-like structures (and associated mitochondria-transfer) in a

bioprinted cancer cell model support the notion that TNT assembly is not associated with culture conditions in 2D settings. Moreover, this system offers an unique opportunity for deeper studies of these communications in controlled and reproducible 3D models to disentangle utmost importance aspects of cancer, such as drug resistance acquisition and other metabolic and molecular processes involved in cancer progression [25,26].

Journal Pre-proof

## 2. Materials and methods

### 2.1. Materials

Gelatin, from porcine skin (CAS no. 9000-70-8), sodium alginate (CAS no. 9005-38-3) and calcium chloride (CAS no. 10035-04-8) were purchased from Sigma-Aldrich Química S.L., Madrid. Other materials were: collagen type I high concentration from rat tail, (Corning), Minimum Essential Medium Eagle 10x (Sigma-Aldrich), Dulbecco's Modified Eagle Medium (Gibco), sodium bicarbonate 7.5% (Thermo Fisher), and Phosphate Saline buffer (PBS) (Corning).

### 2.2. Biomaterial ink preparation

The intrinsic characteristics of the selected materials prevented a one-pot mixing of the components, as gelatin needs heating for melting and collagen coagulates easily above 37 °C. In that way, we proceed to prepare the bioinks by mixing a collagen-containing culture medium (called part A) with a biomaterial hydrogel made with sodium alginate, type A gelatin and PBS as solvent (part B) (Table 1). Three different volumetric ratios were tested to select the most suitable for bioprinting the models. Part A ingredients were used as purchased measured and directly mixed in a 3 ml Eppendorf. In the exploratory study of the biomaterial inks (performed without cells), simple DMEM was added replacing the cell suspension corresponding volume to have a rheological behaviour and printing results as close as possible to the final cell-loaded inks. Part B formulation was elaborated as follows. Firstly, gelatin was weighted, hydrated with half of PBS quantity, and heated in a  $40 \pm 2$  °C bath. Meanwhile, required amount of sodium alginate was mixed under stirring in the remaining volume of PBS. Once gelatin was totally melted, it was slowly added to the alginate blending and gently mixed until complete incorporation. Then, it was left to rest in a bath during 24 h, wrapped with food grade plastic protective film to let the air bubbles disappear. To prepare the mixtures, corresponding volumes of part A and part B were transferred to printer-compatible syringes (BD 3 ml syringe Luer-Lock™ Tip; Benton, Dickinson and Company, Belgium). Both syringes were joined with a female-female luer lock transfer connector (Aesthetic Group, France) and the contents of each cartridge were gently combined until the ink was homogeneous (**Supplementary data, Fig. S1**). Empty syringe and connector were removed, and plastic caps were screwed in nozzle openings to prevent ink loss. Syringes rested in a  $30 \pm 2$  °C bath until use.

Table 1. Detailed compositions and mixtures

|                        |                        |            |            |
|------------------------|------------------------|------------|------------|
| <b>Part A</b>          | Collagen               | 23% (v/v)  |            |
|                        | MEM (x10)              | 10% (v/v)  |            |
|                        | NaHCO <sub>3</sub>     | 7% (v/v)   |            |
|                        | Cell suspension / DMEM | 60% (v/v)  |            |
| <b>Part B</b>          | Sodium alginate        | 6% (w/w)   |            |
|                        | Gelatin                | 16% (w/w)  |            |
| <b>Mixtures tested</b> | <b>3:1</b>             | <b>1:1</b> | <b>1:3</b> |
| <b>Part A</b>          | 3                      | 1          | 1          |
| <b>Part B</b>          | 1                      | 1          | 3          |

### 2.3. Rheological characterization of the mixtures

Rheological analysis was carried out with a controlled stress rheometer (Discovery HR-2, DHR, TA instruments, USA) equipped with a parallel plate (25 mm diameter, 0.5 mm gap) and a controlled convection/radiant heating oven for stable temperature control (Environmental Test Chamber, ETC, TA Instruments, USA). Inks were maintained in a 25 °C bath until testing and were loaded using a plastic spatula. Conditioning steps (30 s) were added prior to every assay to ensure correct sample temperature. Shear-viscosity tests were conducted in flow ramp mode with an increasing shear rate (from 0.01 to 100 s<sup>-1</sup>) within 120 s at 25 °C. Thixotropy at same temperature was measured through a shear recovery test with 3 different steps: 120 s at low shear rate (0.4 s<sup>-1</sup>), 40 s at high shear rate (100 s<sup>-1</sup>) and finally, 120 s at low shear rate (0.4 s<sup>-1</sup>). Structural recovery of the inks was determined as the percentage of viscosity obtained during the first 40 s and the 120 s in the third step, based on the equilibrium viscosity (the average viscosity obtained in the last 40 s of the first step). Small-amplitude oscillatory shear (SAOS) tests were used to study the viscoelastic behaviour of the inks. First, linear viscoelastic interval (LVR) was determined with amplitude sweeps in a 0.1 to 1000% strain interval at 1 Hz. Frequency sweeps were performed from 0.1 to 10 rad/s at a constant deformation of 1% (value within the LVR region). Curves were plotted with average data of three replicates of every assay. Results were recorded and processed by TRIOS software (version 4.5.0, TRIOS Rheology Software, TA Instruments, USA).

#### 2.4. Gcode generation and 3D printing setup

A syringe-based extrusion 3D printer (bIDO-I, Idoma Technological Center, Spain) was used to print the constructs. A flat disk 3D model (15 mm diameter, 0.5 mm height) was imported into an open-source slicing software (Slic3r), from which different versions of G-code were exported depending on the printing parameters set. To select a suitable printing speed, simple squares were printed by triplicate at three different speeds (5 mm/s, 10 mm/s and 15 mm/s). Uniformity and thickness of the printed struts were measured to assess the most appropriate. Other fixed main printing parameters were: 0.15 mm layer height, 60% infill density, 90° infill angle and single perimeter. An extended list of printing parameters is included in Supplementary data. Simple skirt printing was set to establish continuous ink flow before printing. Extruder temperature and printing bed temperature were maintained in 25 °C and 14 °C, respectively, to achieve a correct ink flow without exceeding thermal stress to the cells. Stainless steel, blunt end dispenser tips (Fisnar, United Kingdom) with 0.25 mm inner diameter (25G) were used as printer nozzles. 35 mm sterilized dishes (µ-Dish 35 mm, low wall, ibiTreat; ibidi GmbH, Germany) were chosen as printing supports, since they allowed easy handling, direct microscopic analysis, ensure sterility and hinder evaporation when totally closing the lid.

#### 2.5. 3D printing of preliminary models and cell seeding

For preliminary cell seeding into the selected biomaterial ink, two 3D model configurations were tested. First model printed was a common scaffold, with same porosity in every layer (**Fig. 1A**). Second model, instead, had a bottom solid layer (100% infill density) followed by common porous scaffold layers (**Fig. 1B**). Setting these two models was useful to determine whether the cells adhere to the solid hydrogel layer and/or to the plate surface. Detailed images of the 3D structures' Slic3r preview can be seen at Supplementary data (Fig. S2).

Once printed, constructs were soaked with a 0.5% (w/v) CaCl<sub>2</sub> solution for 2 minutes to allow alginate crosslinking. After that, CaCl<sub>2</sub> solution was removed and scaffolds were gently washed with PBS to remove possible excess of salts. Then, 5x10<sup>4</sup> SCC38 cells or 2.5x10<sup>4</sup> 786-O cells were seeded on the top of the scaffolds and incubated under regular cell culture conditions for 72 hours.

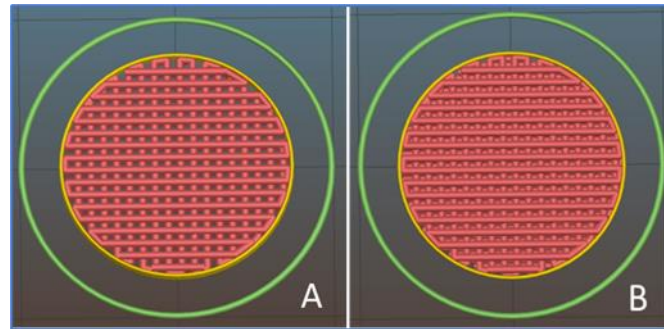


**Fig. 1. Slic3r software preview of 3D models.** (A) Regular scaffold: traditional meshes with struts deposited forming an angle of 90 degrees with the next layer; (B) Scaffold with bottom solid layer: structures where the first layer of the scaffold is printed with 100% infill density, followed by a 90-degree mesh printed.

## 2.6. Bioink preparation and 3D printing process

Part A, containing  $2 \times 10^6$  cells, was immediately transferred into a 3 mL syringe and subsequently mixed with 1.5 mL of the previously prepared part B hydrogel until homogenization. Cell-laden bioinks were kept in a  $30 \pm 1^\circ\text{C}$  bath until printing. Bottom solid layer scaffold (**Fig. 1B**) was selected as 3D model for allowing a better observation of the cells along the different layers. After printed, scaffolds were crosslinked with 0.5% (w/v)  $\text{CaCl}_2$  solution for 2 minutes and then washed with PBS. Finally, DMEM containing 10% of fetal bovine calf serum, penicillin (100 U/mL) and streptomycin (100  $\mu\text{g}/\text{mL}$ ) was added as culture media.

## 2.7. Cell culture and transfection

The clear cell renal cell carcinoma (786-O) and larynx-squamous cell carcinoma (SCC38) cell lines were grown in 10 cm diameter plates in a humidified incubator ( $37^\circ\text{C}$ , 5%  $\text{CO}_2$ ) with DMEM containing 10% of fetal bovine calf serum, penicillin (100 U/mL) and streptomycin (100  $\mu\text{g}/\text{mL}$ ). The SCC38 cell line was kindly provided by Dr R. Grenman and the 786-O cell line was a generous gift from Dr M. Calzada. Cell lines were periodically tested for human pathogens and mycoplasma infection. All methods were carried out in accordance with the approved guidelines of our institution.

For lentiviral infection,  $2.5 \times 10^7$  cells were transiently co-transfected with lentiviral packaging mix and GFP-pGIPZ (Dharmacon) plasmid using Lipofectamine 3000 reagent. The virus-containing media was collected 48 h post-transfection and immediately used to infect 786-O cells in the presence of  $6 \mu\text{g}/\text{mL}$  of polybrene. The infection procedure was repeated 24 hours later. Selection of GFP-expressing cells was performed with  $6 \mu\text{g}/\text{mL}$  of puromycin for 10 days. Stable pooled populations of cells were maintained in culture using  $2 \mu\text{g}/\text{mL}$  of puromycin.

## 2.8. Cell viability

Cell viability was analysed with the Live/Dead viability/cytotoxicity kit (Thermo Fisher) following manufacturer's instructions. Briefly, cells were incubated with  $2 \mu\text{M}$  calcein AM and  $4 \mu\text{M}$  ethidium homodimer-1 in PBS for 30 minutes at  $25^\circ\text{C}$  before microscope visualization using fluorescein and rhodamine optical filters to visualize calcein- (live cells) and ethidium homodimer-1- (dead cells) stained cells.

## 2.9. Fluorescent cell labelling and immunofluorescence

For in vitro mitochondria labelling, cells were incubated with MitoTracker® Red CMXRos (Thermo Fisher) for 30 minutes and then extensively washed with cell culture media following manufacturer's instructions. For immunofluorescence, mouse anti- $\beta$ -actin and mouse anti- $\alpha$ -

tubulin (Sigma-Aldrich, St Louis, MO, USA) were used at 1:500 dilution; rabbit anti-LAMP-1 (Abcam, Cambridge, UK) and rabbit anti-LC3B (Novus Biologicals, Colorado, USA) were used at 1:100 dilution. Anti-rabbit or anti-mouse IgG Alexa Fluor 488 and anti-mouse IgG Alexa Fluor 555 were used as secondary antibodies at 1:500 dilutions. Mounting medium containing DAPI was added to visualize nucleus. Immunofluorescence stainings were analysed on a Zeiss AxioObserver Z1 microscope (Carl Zeiss, Oberkochen, Germany) with a Plan-Apochromat 40X/1.3 (NA = 1.3, working distance = 0.21 mm) or Plan-Apochromat 63X/1.4 (NA = 1.4, working distance = 0.19 mm) oil lens objective, a camera (AxioCam MRm; Carl Zeiss), and Apotome (ApoTome 2; Carl Zeiss) as previously described.

### 2.10. TnT-like structures quantification

Quantifications of TnT-like structures were achieved by using bright field or fluorescence microscopy in life-cells or fixed-cells. For estimations of TnT percentages, cells were pictured using  $8 \times 8$  tiles.

## 3. Results

### 3.1. Rheological characterization and selection of biomaterial ink

Different rheological tests were carried out for a first printability assessment of the inks and to determine the more suitable mixture A:B for bioprinting the models. Flow curves (**Fig. 2A**) showed a greater shear-thinning behaviour when higher content of part B hydrogel was present in the composition. By contrast, 3:1 mixture had a practically Newtonian behaviour, represented by straight lines for both stress ( $\sigma$ ) and viscosity ( $\eta$ ) whose remained constant independently of the shear rate ( $\dot{\gamma}$ ) value.

Regarding the shear recovery tests, neither of the mixtures quickly recovered the gel internal structure after a high shear rate ( $100 \text{ s}^{-1}$ ) at  $25^\circ\text{C}$  (**Fig. 2B**). Similar percentages were found for 1:1 and 1:3 formulas: around 35% and 50% of viscosity recovery, for 40 s and 120 s after the high shear rate step, respectively (**Fig. 2C**). Percentages were even lower for 3:1 ink. These results revealed that, once extruded, the fluids take a long time to recover and that some external help was needed to assist shape retention and preventing them from spilling onto the surface due to gravity. In this vein, taking advantage of the fact that gelatin generates thermo-reversible hydrogels, this weak point was overcome by applying a low temperature in the printing bed and inducing an in-situ instant gelation of the ink.

In SAOS test, LVR was first determined through amplitude sweeps to ensure that tests were carried out without destroying internal structure of the inks (**Supplementary data, Fig. S3**). Constant deformation of 1% was set for frequency sweeps, which display the viscoelastic response of the mixtures (**Fig. 2D**). Every mixture exhibited a typical weak-gel behaviour since storage modulus ( $G'$ ) values were higher than loss modulus ( $G''$ ) values in the three formulations. In addition, higher  $G'$  values (related with better self-supporting ability and larger mechanical strength of the gel) were found for 1:1 mixture. Following all the results, the volumetric ratio selected for bioprinting the 3D models was 1:1 due the more favourable viscoelastic properties and the shear-thinning behaviour.

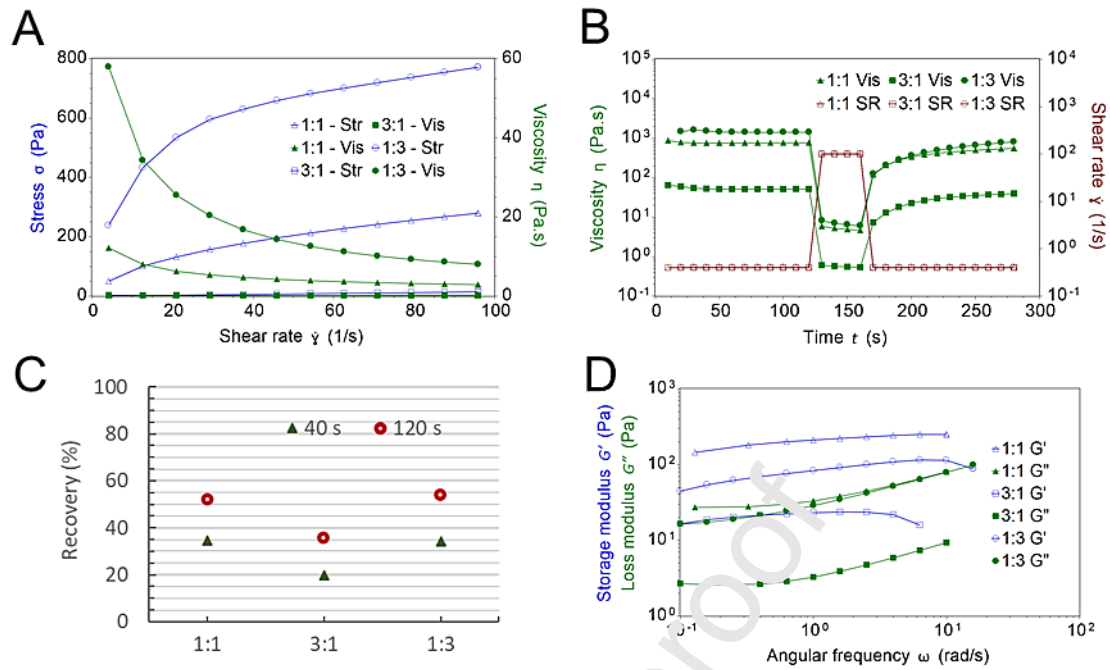


**Fig. 2. Rheological tests.** (A) Shear stress and viscosity profiles from 0.01 to 100  $\text{s}^{-1}$  within 120 s at 25 °C. (B) Shear-recovery test for inks thixotropy evaluation and (C) percentage of viscosity recovery 40 s and 120 s after a high shear rate. (D) Frequency sweeps showing storage modulus ( $G'$ ) and loss modulus ( $G''$ ) of the inks at 25 °C.

### 3.2. 3D printing process

To set the most suitable printing speed, a simple printing test was carried out with the selected ink at different velocities. A speed of 10 mm/s was established for the greater definition in the lines with less deviation (Fig. 3A). The photo image and stereomicroscopic micrograph showed regular pores and struts in the printed scaffolds (Fig. 3B-C). Both model configurations (scaffold with/without bottom solid layer) showed repeatable results.

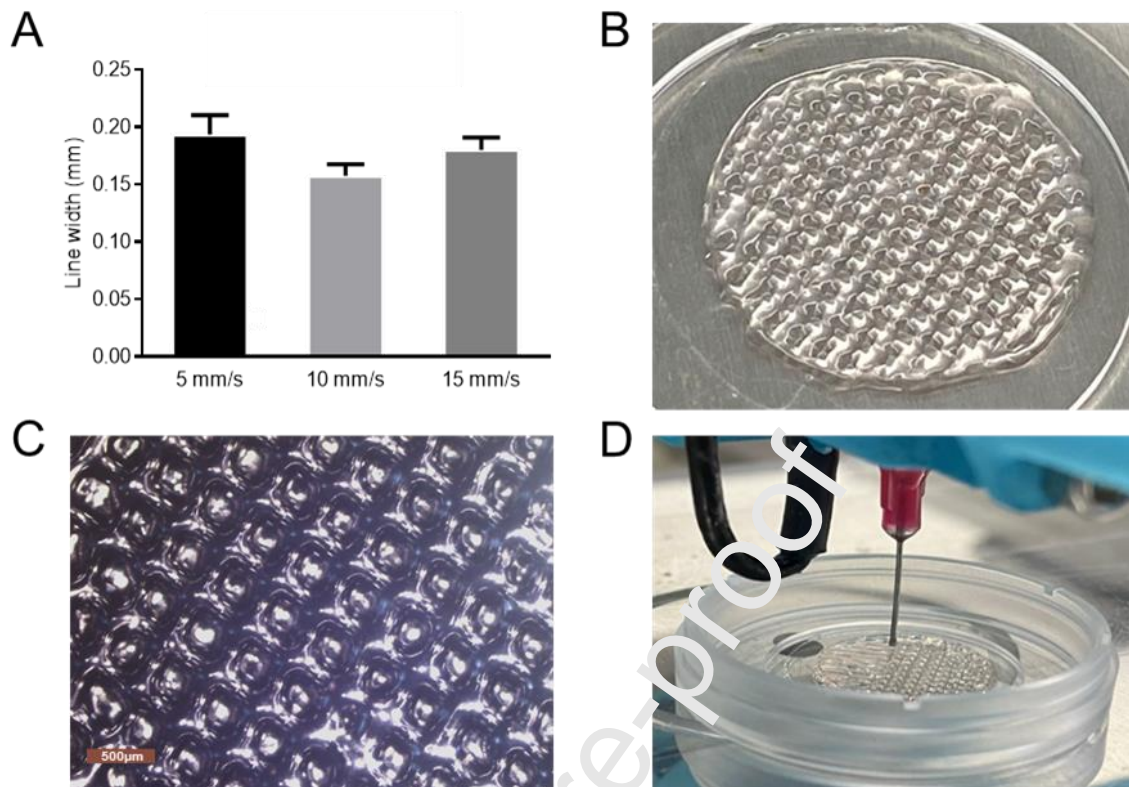


**Fig. 3. Scaffold 3D printing.** (A) Histogram showing line width measurement of bioprinted scaffold printed at 5, 10 and 15 mm/s. Photographs taken with camera (B) and stereomicroscope (C) showed regular pore size and line width. Scale bar: 500  $\mu$ m. (D) Printing process detail.

### 3.3. Viability and proliferation of cancer cells seeded in printed scaffolds

To determine whether cancer cells are viable and retain their ability to proliferate in the presence of biomaterial inks, two different types of scaffolds were used: (i) regular scaffolds printed on culture plates with glass bottoms and (ii) scaffolds printed with a bottom hydrogel solid layer. Two types of cancer cells, 786-O and SCC38, derived from renal cancer or squamous cell carcinoma, respectively, were seeded on the top of the scaffolds and subsequently incubated under regular cell culture conditions for 72 hours. As shown in **Fig. 4A**, both types of cells adhered to the plate coverslips establishing contacts with the hydrogel-boundaries when seeded in regular scaffolds and showing that there is certain cellular tropism towards the hydrogel. Adhered cells spread, i.e., became flattened on the 2D glass substrate indicating that they maintained active polymerization of actin filaments which is the driving force that pushes the membrane forward and allows the motility processes of cancer cells. Moreover, cells proliferated and occupied the whole glass surface after 48 h of culture.

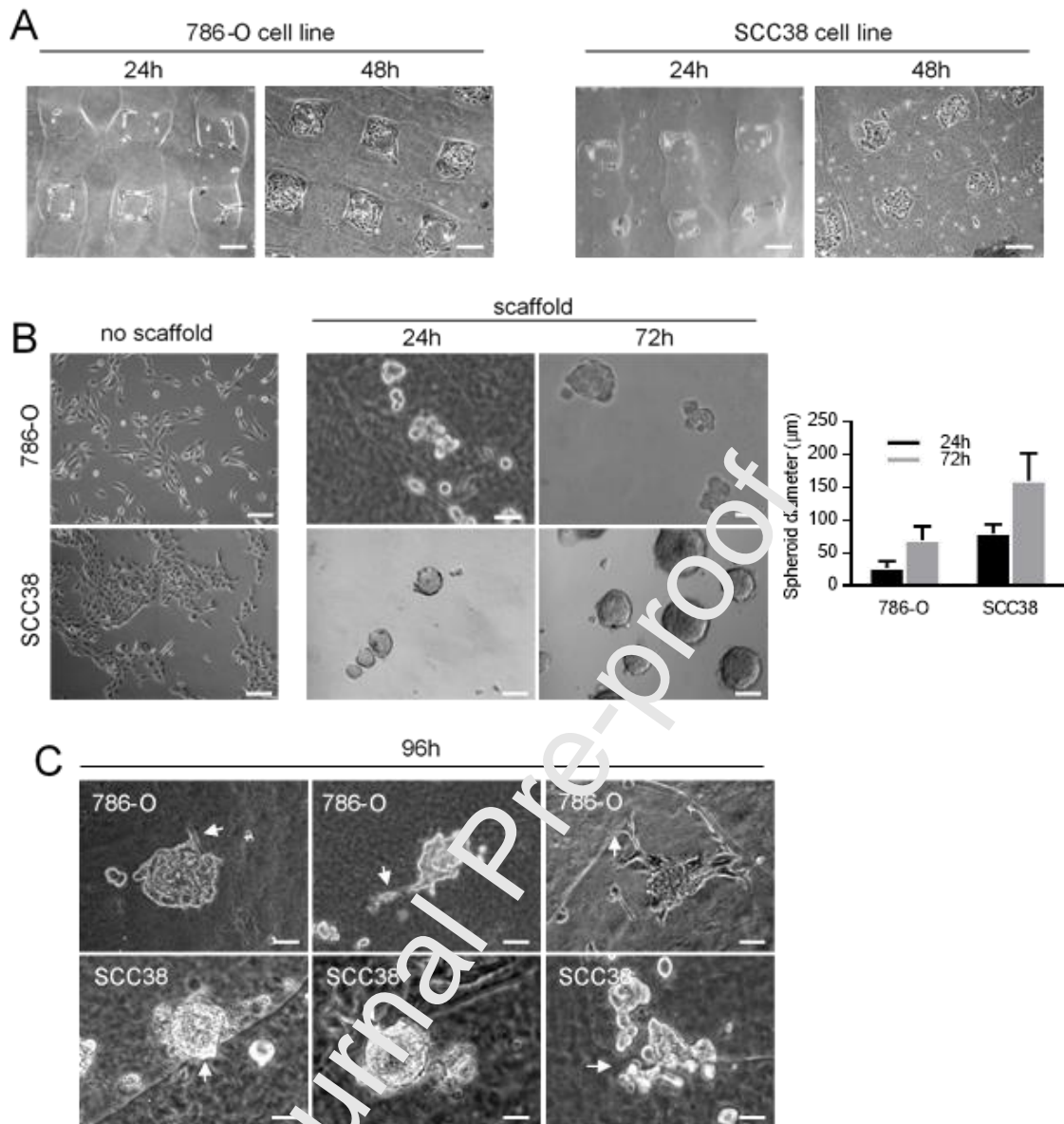


**Fig. 4. Cancer cells are viable and proliferate as multicellular spheroids when seeded on the top of bioink surfaces.** 786-O and SCC38 cells were seeded on top of regular scaffold (A) or scaffold with bottom solid layer (B –right pictures–, and C) and incubated for the indicated periods of time (h, hours). In panel B (left pictures), cells were seeded in regular culture plates to highlight that, under these conditions, cells growth as monolayers adhered to the plate surface. Bar chart on the right represent spheroids diameters in the indicated cells growth on top of scaffold with bottom solid. (C) Representative images of 786-O and SCC38 cells seeded on the top of scaffold with bottom solid layer and subsequently incubated for 96 h. As shown, that the two types of cells are capable of invading the bioinks (white arrows point to invasive cells). Scale bars: 500  $\mu\text{m}$  (A), 100  $\mu\text{m}$  (B, except for top middle and right pictures: 50  $\mu\text{m}$ ) and 50  $\mu\text{m}$  (C).

Different cell behaviour was found when cells were cultured on scaffolds with bottom solid layer. As reported for other types of hydrogels, cells did not growth as monolayer but self-assembled forming 3D multicellular spheroids (MCS) (Fig. 4). SCC38 cells formed larger MCS (mean diameter: 70-90  $\mu\text{m}$ ) than 786-O cells (mean diameter: 20-35  $\mu\text{m}$ ) after 24 h of incubation. In addition, whereas SCC38 cells formed regularly shaped MCS, those assembled with 786-O cells were more amorphous showing less cohesiveness between cells. MCS doubled their size in a 48 h period indicating that cells retained their ability to proliferate (Fig. 4B). More interestingly, both types of cells showed an invasive behaviour penetrating the hydrogel (Fig. 4C). These behaviours resembled those observed when SCC38 and 786-O cells were

assembled into collagen matrices using the classical hanging drop technology [27,28] (**Supplementary data, Fig. S4**). Thus collagen/alginate/gelatin hydrogels are suitable for cancer cell bioprinting and seem to properly mimic the extracellular matrix such that they allow cell adherence and proliferation to assemble multicellular spheroids.

#### 3.4. Viability and proliferation of bioprinted cancer cells

786-O cells were embedded into hydrogels and printed as scaffolds with bottom solid hydrogel layers. In this setting, printed cells scattered as single cells within the hydrogel. Bright-field microscopy allowed visualization of cells within the scaffolds. To better distinguish cells, a stable population of 786-O cells expressing green fluorescent (GFP) protein was generated. These cells were mixed with the hydrogel and subsequently bioprinted as indicated above. **Fig. 5** shows that individual cells could be visualized in- or out-of focus indicating they are at different Z-positions within the hydrogel. The number of cells doubled after about 15 days of culture indicating that bioprinted cells do proliferate with lower rate than not-bioprinted cells, thus more closely resembling native cancer cell behaviour. It takes about three to six months for most tumours to double their size [29].

Bioprinted cancer cells could be cultured for long periods of time and remained viable during that time (over 15-20 days). Cell viability was analysed by using calcein and ethidium bromide to stain live (green) or dead (red) cells in cells not expressing GFP. As shown in Fig. 5, about 90% of bioprinted cells remained viable after 15 days of culture. In addition, single bioprinted cells seem to retain fluid dynamic and intracellular movements of the complex constituents of the cytoplasm, an intrinsic property of cells which is vital for regulating relevant physiological events. Intracellular dynamic movements were detected in single bioprinted cells by the time-lapse recordings (see Supplementary data, video 1).

#### 3.5. Assembling of TNT-like structures in 786-O cells cultured as monolayers and bioprinted models

TNT-like connections have been spotted in different types of cancer cells, including SCC38 cells, when they are grown as monolayers, but there is no evidence for the existence of TNT-like structures in cells derived from renal cancer. Moreover, it is unknown whether bioprinted cancer cells retain their ability to assemble TNT-like projections within hydrogels. Side-by-side bright-field microscopic analysis of SCC38 and 786-O cells unveiled that 786-O cells can assemble a remarkable higher number of cell-to-cell long projections than SCC38 cells and other SCC-derived cells [25] (**Supplementary data, Fig. S5**). Thus, subsequent studies were focused on 786-O cells to ascertain whether they retained their ability to assemble functional TNT-like projections with the aim of providing a highly accessible, more physiological, controlled and reproducible 3D model than the 2D culture system or tumour tissues.

A first analysis was performed in cells cultured under conventional 2D planar culture conditions. As shown in **Fig. 6**, 786-O cells grown as 2D monolayers generated thin tube structures that connected distant cells forming membrane bridges. Immunostainings of  $\alpha$ -tubulin and  $\beta$ -actin showed that both cytoskeleton proteins were localized inside the cell projections. Immunofluorescence analysis using anti-LAMP1 and anti-LC3B antibodies, as lysosome and autophagosome markers, respectively, revealed that the two types of subcellular organelles were present in the cell projections. Moreover, cell labelling with mitotracker showed that they also contained mitochondria which were able to travel inside the channel. The average migration rate of mitochondria was about 30  $\mu\text{m}/\text{h}$  which was similar to that described in other cancer cells [26].

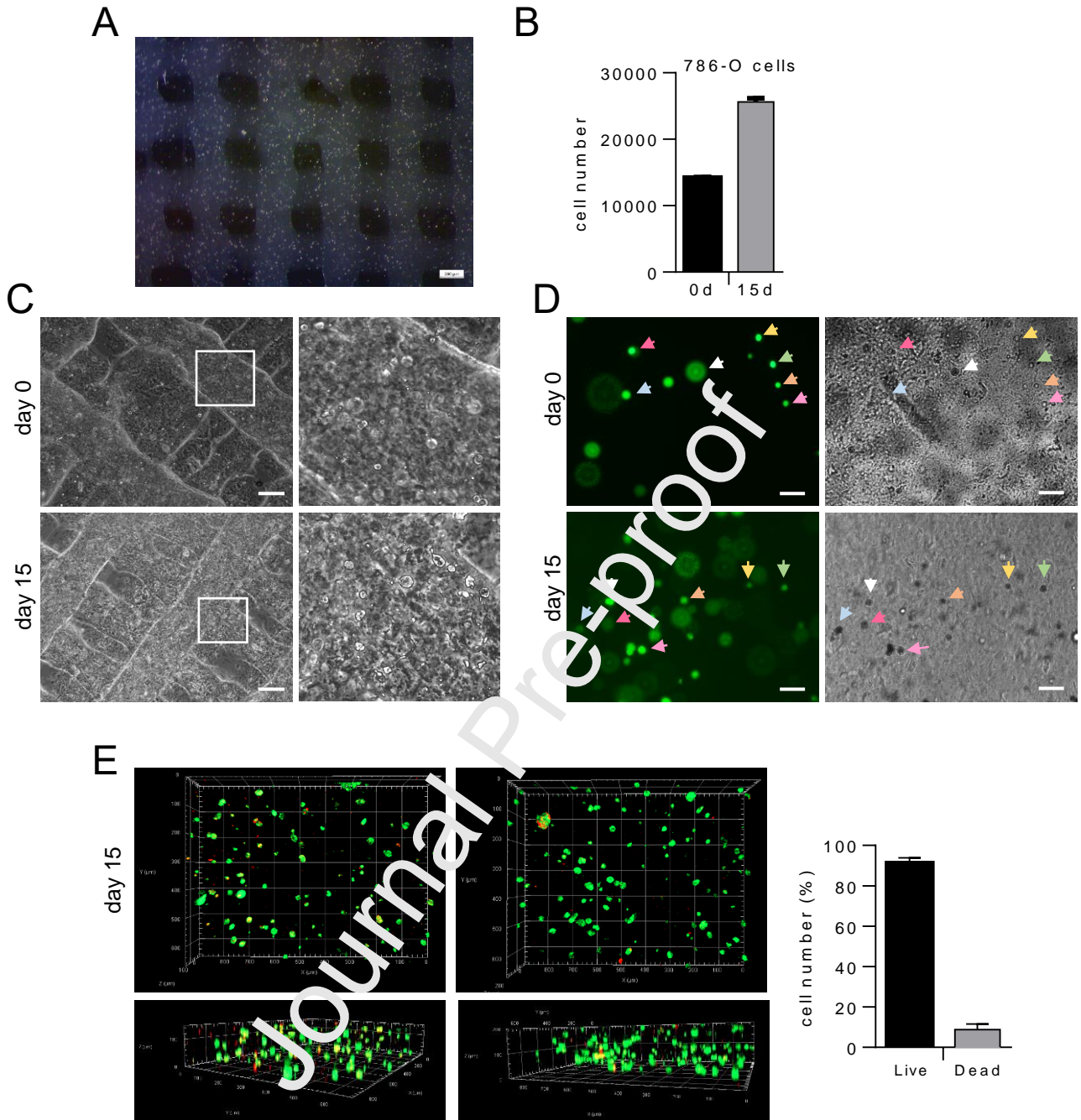


**Fig. 5. Bioprinted cancer cells are viable and proliferate over long periods of time.** 786-O cells were embedded into the bioink, printed as scaffolds with bottom solid layer and photographed either immediately after printing or after incubation for 15 or 20 days. (A) A representative image showing an overview of the scaffold structure and the printed cells (bright dots) after 20 days of incubation. (B) Quantification of the number of cells immediately after printing (0 d) or after 15 days (15 d) of incubation. (C-E) Representative images of printed scaffolds photographed immediately after printing (day 0) or after 15 days of incubation. In panel C, magnified images of the framed areas are shown. (D) 786-O cells were stably transfected with GFP protein before printing in the scaffolds to obtain better visualization of printed cells. Images show microscopic fluorescence and brightfield pictures of the same region of the scaffolds. Arrows point to individual cells expressing GFP protein. As shown, there are cells out of focus because of their location at different z positions. (E) Printed cells were incubated for 15 days and subsequently stained with Live-Dead Assay Kit which label live and dead cells in green and red, respectively. The percentage of cells was estimated from a total of 340 cells counted in 4 independent experiments. Images were captured using fluorescence microscopy and represent a stack of 15 sections with a total physical length of 140  $\mu\text{m}$  (left panel) or 20 sections with a total physical length of 190  $\mu\text{m}$

(right panel). xy (upper pictures) and xz (lower pictures) projections of the same scaffold are shown. Scale bars: 500  $\mu\text{m}$  (A, C); 100  $\mu\text{m}$  (D).

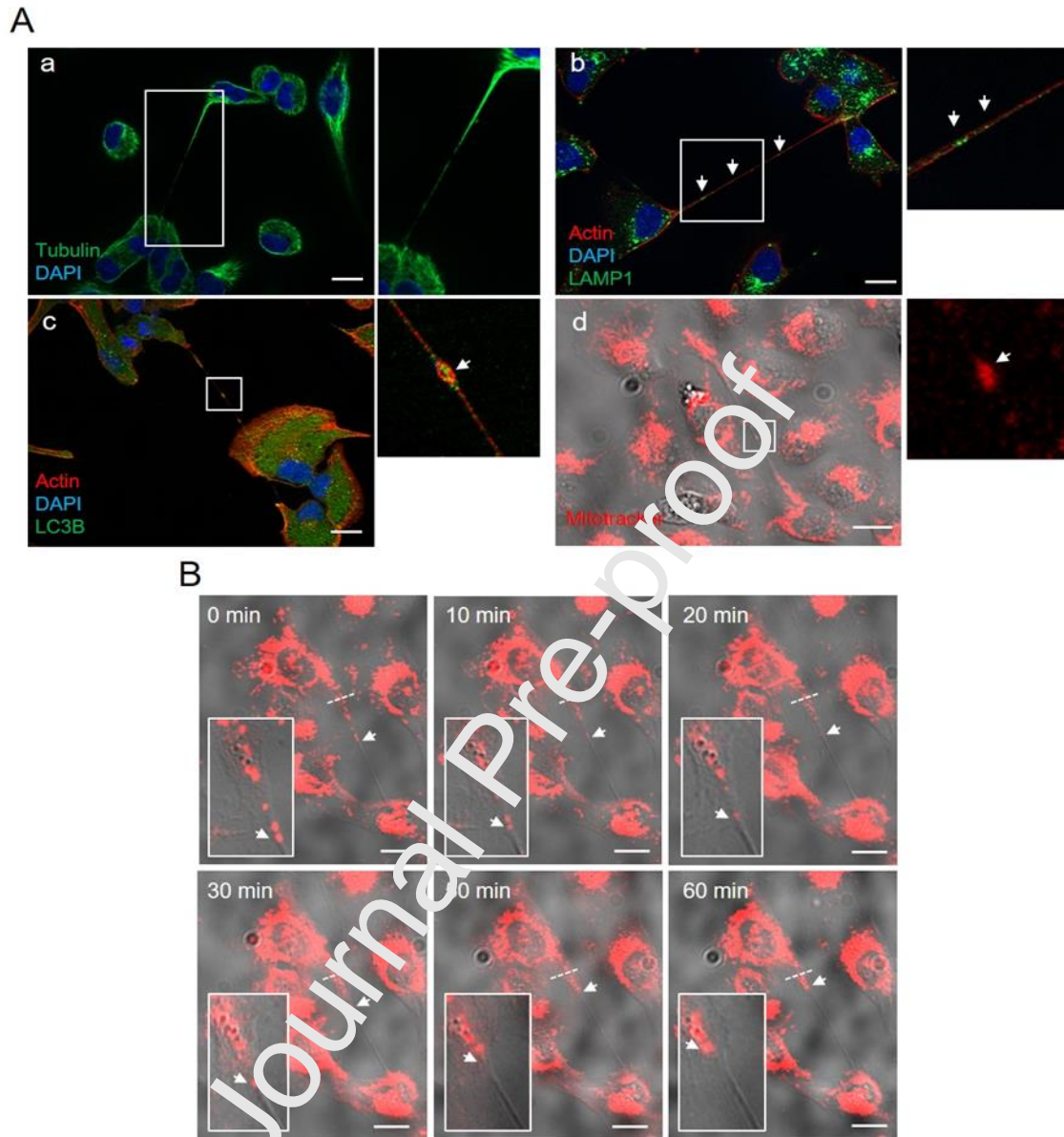


**Fig. 6. TNT-like structures formed by 786-O cells grown as monolayers and mitochondria trafficking.** (A) a-c Representative fluorescence microscopic images of cells stained for tubulin, actin, LAMP1 and LC3B as indicated in each picture. Cell nuclei are stained with DAPI in blue. (d) Representative merged transmitted light and fluorescence images of cells labelled with mitotracker (red). Magnified images of the framed areas are shown to better visualize lysosomes (b), autophagosomes (c) and mitochondria (d) inside the TNTs. White arrows point to the different organelles. (B) Representative merged transmitted light and fluorescence images from time-lapse movies at the indicated times. 786-O cells were labelled in vitro with red mitotracker. White arrows point to the migrating mitochondria. Dashed white lines highlight one of the two the endpoints of the TNTs taken as a reference. Scale bars: 20  $\mu\text{m}$ .

To determine whether bioprinted cells retained their ability to assemble TNT-like structures, we first verified that the presence of the hydrogel in a regular cell culturing system did not impair assembling of those structures (**Fig. 7A**). Next, cells were encapsulated in printed scaffolds and subsequently video recorded. **Fig. 7B** shows that printed cells actually assembled TNT-like projections connecting distant cells (see **Supplementary data, video 2**). To determine

whether those structures were functional, the exchange of mitochondria between connected cells via TNT was studied. To this end, GFP-expressing cells were biprinted, cultured for 35 days and subsequently labelled with mitotracker. Biprinted cells were recorded by time-lapse microscopy to register mitochondria movement. **Fig. 8** illustrates the sequence of images over time demonstrating the migration of mitotracker-containing vesicles along the TNTs-like projections with an average migration rate similar to that of cells growth as 2D-monolayer (about 33  $\mu\text{m}/\text{h}$ ).

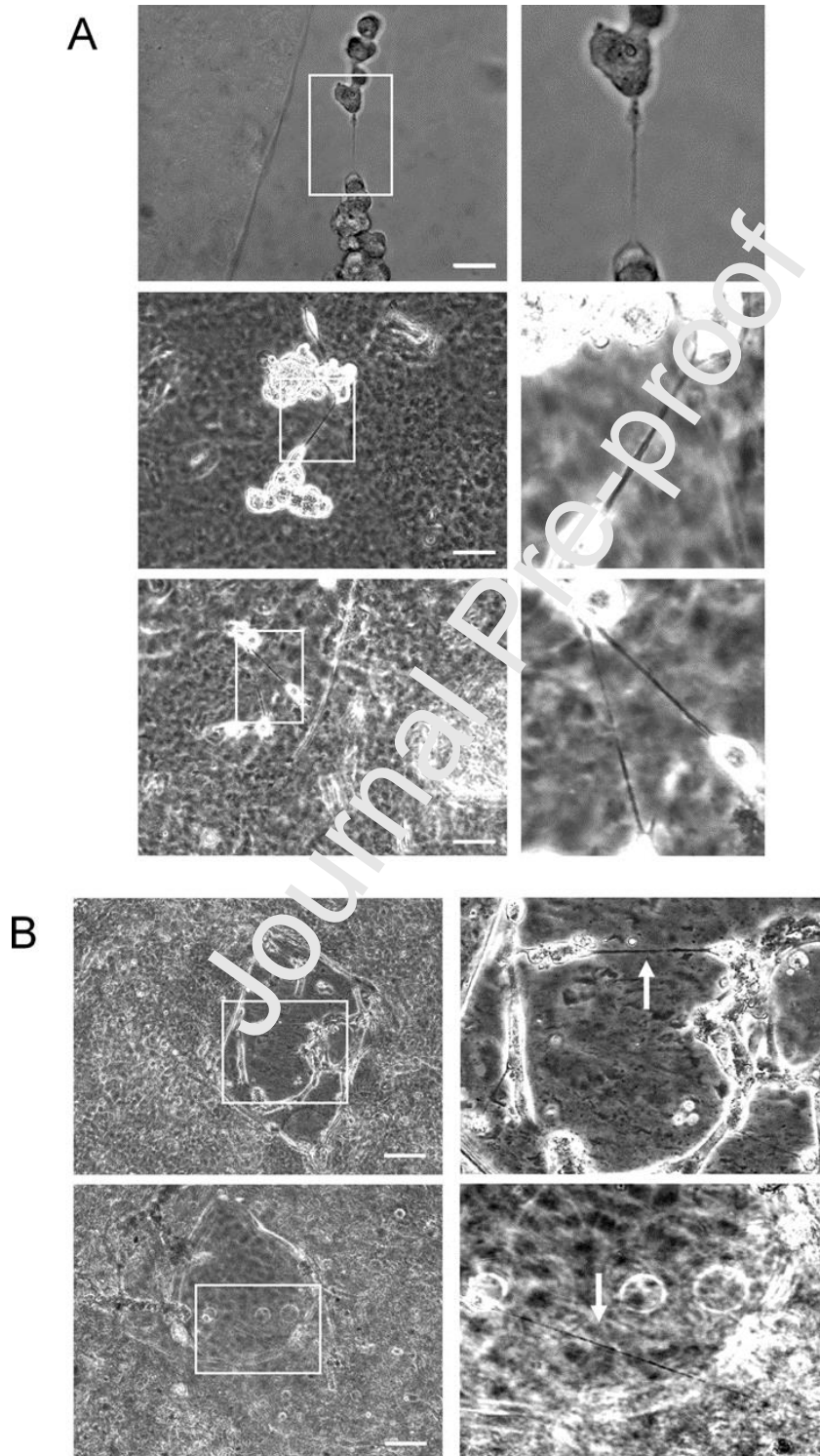
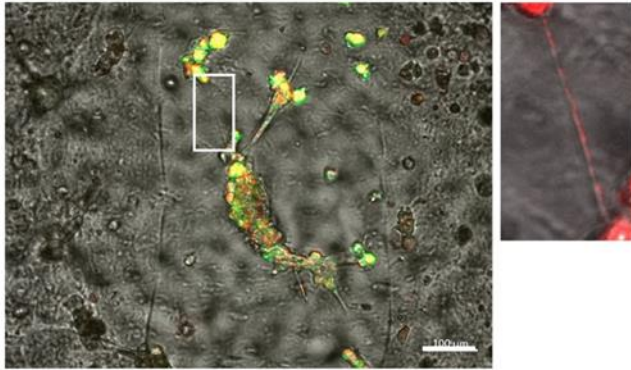


**Fig. 7. Printed 786-O cancer cells retain their ability to form TNT-like structures.** Cells were seeded

on top scaffolds with bottom solid layer (A) or bioprinted (B). White arrows point to TNT-like projections. Magnified images of the framed areas are shown. Scale bars: 50  $\mu\text{m}$  (A), 100  $\mu\text{m}$  (B).

A



B

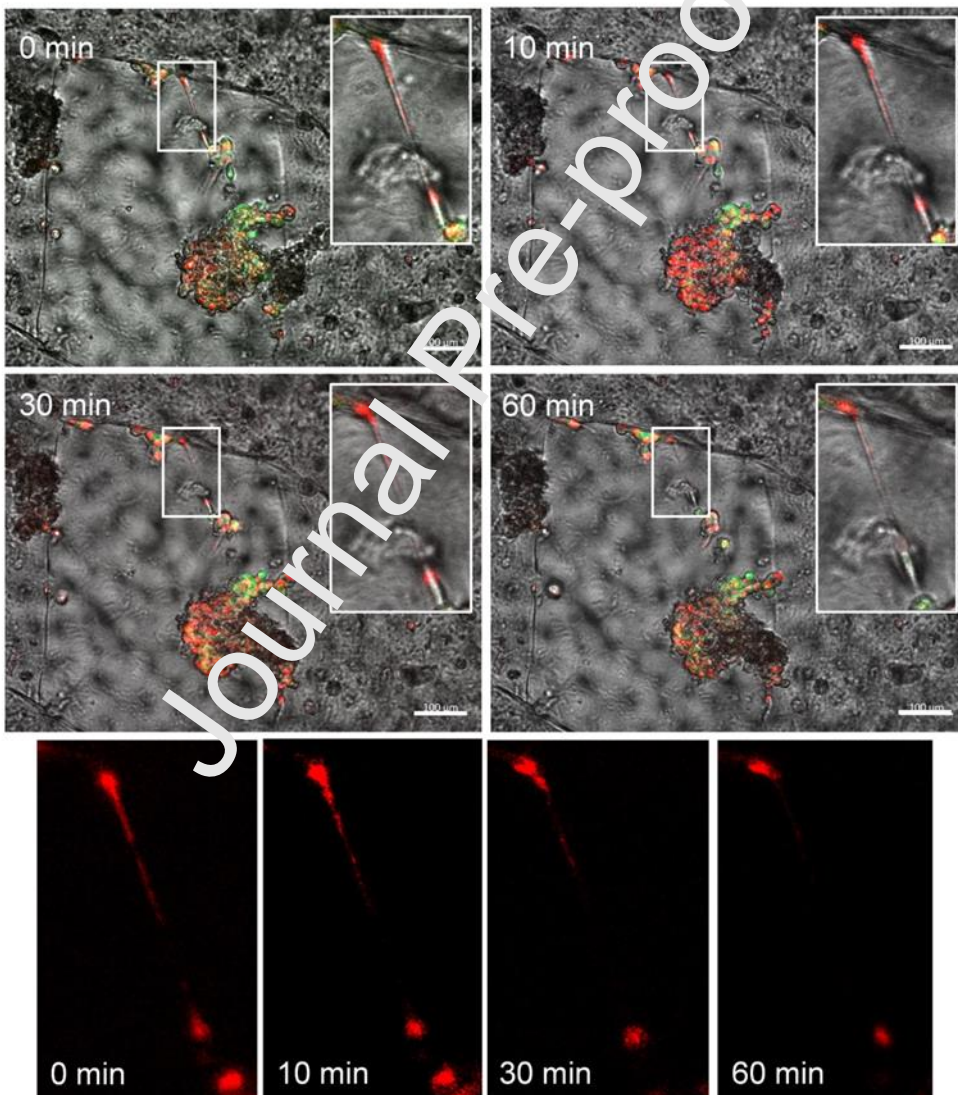


**Fig. 8. Mitochondria trafficking through TNT-like projections in bioprinted 786-O cells.** GFP-expressing 786-O cells were labelled with mitotracker before bioprinting. Bioprinted cells were maintained in culture for 35 days before tracking analysis. Representative merged transmitted light and fluorescence images from time-lapse movies at the indicated time points are shown in A and B. Fluorescence images of the TNT highlighted in B (upper pictures) are shown in the bottom to show the migratory behaviour of labelled mitochondria along the TNT. Scale bars: 100  $\mu\text{m}$ .

#### 4. Discussion

Cell-to-cell and cell-environment interactions are responsible for cell differentiation, proliferation, gene and protein expression, drug metabolism, and other cellular functions that are essential for the multicellular systems. In this study, we explored the creation of three-dimensional bioprinted cell-systems to be used as models for the observation of cancer cell behaviour and communication.

Investigation in bioink composition and rheological behaviour was a major step for the acquisition of successfully bioprinted. Although collagen/gelatin/alginate mixtures have been previously used in 3D bioprinting [30], its application on cancer cell studies has not been established or reported to date. Moreover, appropriate configuration of printing parameters (as layer height, printing speed or infill density) were also indispensable to achieve resistant structures that remained unchanged in time in culture conditions. It is widely accepted that shear-thinning inks are favourable for extrusion-driven bioprinting, since this behaviour allows the fluid to flow easily when passing through a narrow nozzle that increases the shear forces applied to the ink [31–33]. Furthermore, some viscoelastic properties, as self-supporting ability, or sufficient mechanical strength of the gel, are highly desirable to avoid the collapse of the growing 3D object [15,34]. In that way, due to the slow recovery of the mixtures tested, a sol-gel transition effect was induced by keeping the extruder in a free-flow ink temperature and the printing bed in a colder temperature, which caused instant gelation of the bioink when reaching the platform and the generation of an accurate mesh. The chemical crosslinking between alginate and  $\text{Ca}^{2+}$  ions of the  $\text{CaCl}_2$  solution and collagen polymerization under normal culture conditions ( $37^\circ\text{C}$  and neutral pH  $\sim 7.4$ ) [35] helped in achieving strengthened and resistant structures, avoiding swelling and remaining undamaged through long periods of time (up to 31 days).

The use of two different model configurations —scaffold with or without bottom solid layer-, gave us the opportunity to analyse how cancer cells interact with the composite hydrogels. Both, renal- and larynx SCC-derived cells tended to adhere to the glass surface within the scaffold gaps when they were seeded in scaffolds without bottom solid layer. Remarkably, although cells did not adhere to the hydrogel, they initially established contacts with it, being placed in the boundaries of the scaffold windows thus indicating that there is certain cell tropism for the hydrogel components. Further, these cells spread, proliferated in the scaffold windows, and even penetrated the scaffold thus showing that they retained proliferative and invasive properties. By contrast, cells seeded on scaffolds with bottom solid layer formed MCS. The MCS generated under these conditions were highly similar in morphology and growth rate to those formed by the classical hanging drop protocol. This demonstrates that, under these culture conditions, the two types of cancer cells tested retain the intrinsic property of self-aggregation which is typical of cancer cells [36]. These MCS resemble pseudo-tumours and constitute one of the most reliable models for cancer research since, as opposed, cells cultured in 2D adhered to the culture plate, MCSs faithfully recapitulate cancer cell behaviour in complex organisms. Therefore, the designed hydrogels are suitable for the assembly of MCS of renal- and SCC-derived cells and provide a valuable setting for studies of pathologically relevant cancer cell phenotypes. Observing that two cancer cells lines derived from unrelated type of cancers show similar behaviour, suggest that the model could be more broadly implemented in research of other types of cancer. A handicap of this model, however, is the lack of cell-extracellular components interactions, which was overcome directly bioprinting scaffolds with embedded cells.

In that sense, the bioprinting settings and hydrogel composition described are useful as proof-of-concept model that allow cancer cell bioprinting and the observation of direct cell-to-cell communication via TNT-like protrusions. It also provides evidence that mitochondria, the cell's

energy-generating structures, scroll through TNT-like projections. However, additional approaches will be required to definitively demonstrate whether these and/or other organelles are transferred from one cell to another via those projections. TNT-like structures and transferring of diverse cargo have been described in different types of cancer cells [8] but, to the best of our knowledge, they have not been previously spotted in renal cancer cells. According to recent reports [37], the cell projections identified in 786-O cells fulfil criteria to be defined as TNTs-like structures.

They are actin-containing structures that establish continuous membrane connections between cells, do not adhere to substratum, and transport mitochondria. Importantly, these structures were not only detected in 2D cultured cells and MSCs but also in bioprinted cells. This indicates that TNT-like projections are not an artefact caused by the features inherent to cell cultures such as the artificial adhesion of cells to plastic/glass surfaces and lack of cell-extracellular components interactions. They can be assembled inside a complex 3D structure, connect distant cells, and enable mitochondria trafficking.

The role of TNT-like structures in cancer is still under active investigation [10]. While they have been identified in many types of cancer cell cultures using light microscopy [8], their detection in more complex contexts, such as tumour tissues, is still challenging due to their scarce molecular characterization and the high cellular density of the tumour tissues. Similar disadvantages emerge when trying to identify TNT-like structures within MCSs where cells are very densely packed. These are major handicaps for the functional characterization of TNT-like structures in cancer and other diseases. Therefore, controlled and highly reproducible 3D models are urgently needed to design the experimental approaches required for the understanding of the role of TNT-like structures in cancer progression and drug resistance, and exploit this knowledge for improving cancer treatment options. The integration of bioprinting methods and microscopic analysis of TNT-like structures connecting distant cells within 3D matrices, offers now the opportunity of exploring the role of these unconventional ways of communications between cells in cancer and many other diseases in a controlled 3D microenvironment.

## 5. Conclusions

We report here a 3D bioprinted cancer model for the investigation of intercellular communication, via TNT-like structures, in a highly controlled and reproducible environment resembling the *in vivo* tumour ecosystem. This technology uses an optimized collagen/alginate/gelatin hydrogel and optimized printing parameters to bioprint renal cancer cells. In this context, cells are viable, proliferate for long-time periods of time, and form long and thin TNT-like structures that are used as channels for the long-distance cell-to-cell transfer of mitochondria. Identification and functional analysis of TNTs in complex contexts, such as tumor tissues or multicellular spheroids, is still challenging due to the absence of specific biomarkers and the high cellular density. The results reported here establish the potential for bioprinting cancer cells to investigate cancer cell communication via TNTs within a physiologically relevant microenvironment.

## CRedit author statement

**Helena Herrada:** Conceptualization, Methodology, Formal analysis, Investigation, Visualization, Writing- Reviewing and Editing **Lucia Celada:** Methodology, Formal analysis, Investigation, Visualization. **David Rodriguez:** Investigation; Methodology. **M Alejandro:** Conceptualization, Project administration, Supervision. **Enrique Aguilar:** Supervision, Writing- Reviewing and Editing. **María-Dolores Chiara:** Conceptualization, Supervision, Project administration, Funding acquisition, Writing- Reviewing and Editing.

## Conflict of Interest

The authors declare that they have no known competing financial interests or personal relationships that could have appeared to influence the work reported in this paper.

## Acknowledgements

This research was funded by Fondo de Investigación Sanitaria grant number FIS PI20/01754 and the Red Temática de Investigación Cooperativa en Cáncer, CIBERONC, Instituto de Salud Carlos III (ISCIII). L.C. thanks the Spanish Ministerio de Ciencia, Innovación y Universidades for a FPU predoctoral contract.

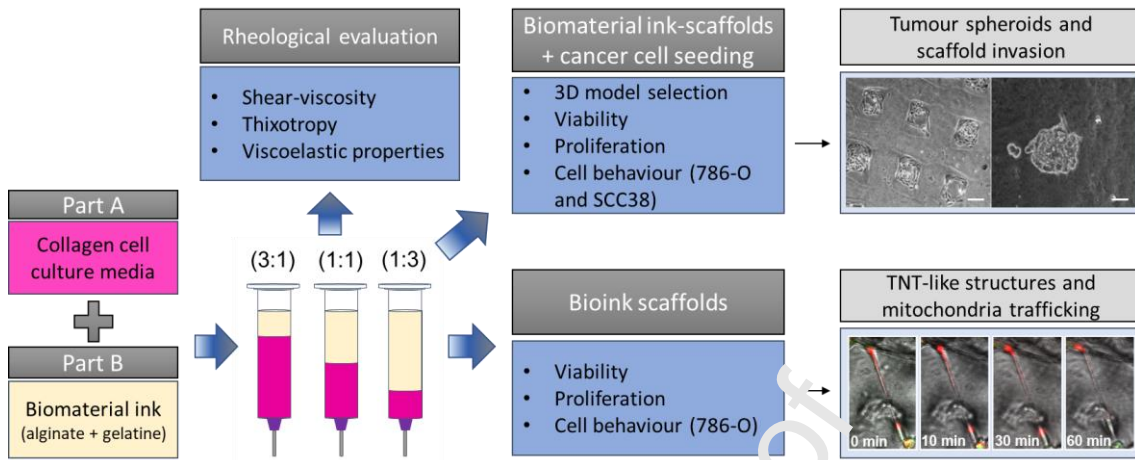
## References

- [1] A.M. Sitarski, H. Fairfield, C. Falank, M.R. Reagan, 3D Tissue Engineered in Vitro Models of Cancer in Bone, *ACS Biomater. Sci. Eng.* 4 (2018) 324–336. <https://doi.org/10.1021/acsbiomaterials.7b00097>.
- [2] F. Pampaloni, E.G. Reynaud, E.H.K. Stelzer, The third dimension bridges the gap between cell culture and live tissue, *Nat. Rev. Mol. Cell Biol.* 8 (2007) 839–845. <https://doi.org/10.1038/nrm2236>.
- [3] R. Edmondson, J.J. Broglie, A.F. Adcock, L. Yang, Three-dimensional cell culture systems and their applications in drug discovery and cell-based biosensors, *Assay Drug Dev. Technol.* 12 (2014) 207–218. <https://doi.org/10.1089/adt.2014.5/3>.
- [4] A. Doctor, V. Seifert, M. Ullrich, S. Hauser, J. Dietrich, Three-dimensional cell culture systems in radiopharmaceutical cancer research, *Cancers (Basel)*. 12 (2020) 1–28. <https://doi.org/10.3390/cancers12102765>.
- [5] D. Herrmann, J.R.W. Conway, C. Vennin, A. Magenau, W.E. Hughes, J.P. Morton, P. Timpson, Three-dimensional cancer models mimic cell-matrix interactions in the tumour microenvironment, *Carcinogenesis*. 35 (2014) 1671–1679. <https://doi.org/10.1093/carcin/bgu108>.
- [6] A.A.A. Al-Juboori, A. Ghosh, M.M. Bin Jamaluddin, M. Kumar, S.S. Sahoo, S.M. Syed, P. Nahar, P.S. Tanwar, Proteomic Analysis of Stromal and Epithelial Cell Communications in Human Endometrial Cancer Using a Unique 3D Co-Culture Model, *Proteomics*. 19 (2019) 1800448. <https://doi.org/10.1002/pmic.201800448>.
- [7] S.A. Langhans, Three-Dimensional in Vitro Cell Culture Models in Drug Discovery and Drug Repositioning, *Front. Pharmacol.* 9 (2018). <https://doi.org/10.3389/fphar.2018.00006>.
- [8] G. Pinto, C. Brou, C. Zurzolo, Tunneling Nanotubes: The Fuel of Tumor Progression?, *Trends in Cancer*. 6 (2020) 874–888. <https://doi.org/10.1016/j.trecan.2020.04.012>.
- [9] A. Rustom, Nanotubular Highways for Intercellular Organelle Transport, *Science (80-. )*. 303 (2004) 1007–1010. <https://doi.org/10.1126/science.1093133>.
- [10] M. Baker, How the Internet of cells has biologists buzzing, *Nature*. 549 (2017) 322–324. <https://doi.org/10.1038/549322a>.
- [11] J.R. Browning, P. Derr, K. Derr, N. Doudican, S. Michael, S.R. Lish, N.A. Taylor, J.G. Krueger, M. Ferrer, J.A. Carucci, D.S. Gareau, A 3D biofabricated cutaneous squamous cell carcinoma tissue model with multi-channel confocal microscopy imaging biomarkers to quantify antitumor effects of chemotherapeutics in tissue, *Oncotarget*. 11 (2020) 2172–2181. <https://doi.org/10.18632/oncotarget.27570>.
- [12] E.M. Langer, B.L. Allen-Petersen, S.M. King, N.D. Kendsersky, M.A. Turnidge, G.M. Kuziel, R. Riggers, R. Samatham, T.S. Amery, S.L. Jacques, B.C. Sheppard, J.E. Korkola, J.L. Muschler, G. Thibault, Y.H. Chang, J.W. Gray, S.C. Presnell, D.G. Nguyen, R.C. Sears, Modeling Tumor Phenotypes In Vitro with Three-Dimensional Bioprinting, *Cell Rep.* 26 (2019) 608–623.e6. <https://doi.org/10.1016/j.celrep.2018.12.090>.

- [13] S. Knowlton, S. Onal, C.H. Yu, J.J. Zhao, S. Tasoglu, Bioprinting for cancer research, *Trends Biotechnol.* 33 (2015) 504–513. <https://doi.org/10.1016/j.tibtech.2015.06.007>.
- [14] A. Mondal, A. Gebeyehu, M. Miranda, D. Bahadur, N. Patel, S. Ramakrishnan, A.K. Rishi, M. Singh, Characterization and printability of Sodium alginate –Gelatin hydrogel for bioprinting NSCLC co-culture, *Sci. Rep.* 9 (2019) 19914. <https://doi.org/10.1038/s41598-019-55034-9>.
- [15] A. Schwab, R. Levato, M. D’Este, S. Piluso, D. Eglin, J. Malda, Printability and Shape Fidelity of Bioinks in 3D Bioprinting, *Chem. Rev.* 120 (2020) 11028–11055. <https://doi.org/10.1021/acs.chemrev.0c00084>.
- [16] I.T. Ozbolat, K.K. Moncal, H. Gudapati, Evaluation of bioprinter technologies, *Addit. Manuf.* 13 (2017) 179–200. <https://doi.org/10.1016/j.addma.2016.10.003>.
- [17] C. Lee, E. Abelseth, L. de la Vega, S.M. Willerth, Bioprinting a novel glioblastoma tumor model using a fibrin-based bioink for drug screening, *Mater. Today Chem.* 12 (2019) 78–84. <https://doi.org/10.1016/j.mtchem.2018.12.005>.
- [18] J. Bae, S. Han, S. Park, Recent Advances in 3D Bioprinted Tumor Microenvironment, *BioChip J.* 14 (2020) 137–147. <https://doi.org/10.1007/s13206-020-4201-5>.
- [19] S. Amorim, D. Soares Da Costa, I. Pashkuleva, C.A. Reis, F.L. Reis, R.A. Pires, 3D hydrogel mimics of the tumor microenvironment: The interplay among hyaluronic acid, stem cells and cancer cells, *Biomater. Sci.* 9 (2021) 252–260. <https://doi.org/10.1039/d0bm00843e>.
- [20] S. Mao, Y. Pang, T. Liu, Y. Shao, J. He, H. Yang, Y. Mao, W. Sun, Bioprinting of in vitro tumor models for personalized cancer treatment: a review, *Biofabrication.* 12 (2020) 042001. <https://doi.org/10.1088/1758-5090/ab97c0>.
- [21] M.G. Sánchez-Salazar, M.M. Álvarez, G. Trujillo-de Santiago, Advances in 3D bioprinting for the biofabrication of tumor models, *Biofabrication.* 21 (2021) e00120. <https://doi.org/10.1016/j.bprint.2020.00120>.
- [22] P. Datta, M. Dey, Z. Ataie, D. Unutmaz, I.T. Ozbolat, 3D bioprinting for reconstituting the cancer microenvironment, *Npj Precis. Oncol.* 4 (2020). <https://doi.org/10.1038/s41698-020-0121-2>.
- [23] B.S. Kim, W. Cho, G. Gao, M. Ahn, S. Kim, D. Cho, Construction of Tissue-Level Cancer-Vascular Model with High-Precision Position Control via In Situ 3D Cell Printing, *Small Methods.* (2021). <https://doi.org/10.1002/smt.202100072>.
- [24] H. Li, S. Liu, L. Lin, Rheological study on 3D printability of alginate hydrogel and effect of graphene oxide, *Int. J. Bioprinting.* 2 (2016) 10–12. <https://doi.org/10.18063/IJB.2016.02.007>.
- [25] Y. Hekmatshoar, J. Naeije, M. Galloni, M.L. Vignais, The role of metabolism and tunneling nanotube-mediated intercellular mitochondria exchange in cancer drug resistance, *Biochem. J.* 475 (2018) 2305–2328. <https://doi.org/10.1042/BCJ20170712>.
- [26] I. Sáenz-de-Santa-María, C. Bernardo-Castiñeira, E. Enciso, I. García-Moreno, J.L. Chiara, C. Suarez, M.D. Chiara, Control of long-distance cell-to-cell communication and autophagosome transfer in squamous cell carcinoma via tunneling nanotubes, *Oncotarget.* 8 (2017) 20939–20960. <https://doi.org/10.18632/oncotarget.15467>.
- [27] C. Bernardo-Castiñeira, N. Valdés, L. Celada, A.S.J. Martinez, I. Sáenz-De-Santa-María, G.F. Bayón, A.F. Fernández, M.I. Sierra, M.F. Fraga, A. Astudillo, P. Jiménez-Fonseca, J.C. Rial, M.Á. Hevia, E. Turienzo, C. Bernardo, L. Forga, I. Tena, M.J. Molina-Garrido, L. Cacho, C. Villabona, T. Serrano, B. Scola, I. Chirivella, M. Del Olmo, C.L. Menéndez, E. Navarro, M. Tous, A. Vallejo, S. Athimulam, I. Bancos, C. Suarez, M.D. Chiara, Epigenetic Deregulation of Protocadherin PCDHGC3 in Pheochromocytomas/Paragangliomas Associated with SDHB Mutations, *J. Clin. Endocrinol. Metab.* 104 (2019) 5673–5692. <https://doi.org/10.1210/je.2018-01471>.
- [28] I. Saéenz-de-Santa-María, L. Celada, M.-D. Chiara, The Leader Position of Mesenchymal Cells Expressing N-Cadherin in the Collective Migration of Epithelial Cancer, *Cells.* 9 (2020) 731. <https://doi.org/10.3390/cells9030731>.

- [29] T.-K. Yoo, J.W. Min, M.K. Kim, E. Lee, J. Kim, H.-B. Lee, Y.J. Kang, Y.-G. Kim, H.-G. Moon, W.K. Moon, N. Cho, D.-Y. Noh, W. Han, In Vivo Tumor Growth Rate Measured by US in Preoperative Period and Long Term Disease Outcome in Breast Cancer Patients, *PLoS One*. 10 (2015) e0144144. <https://doi.org/10.1371/journal.pone.0144144>.
- [30] Z. Wu, X. Su, Y. Xu, B. Kong, W. Sun, S. Mi, Bioprinting three-dimensional cell-laden tissue constructs with controllable degradation, *Sci. Rep.* 6 (2016) 1–10. <https://doi.org/10.1038/srep24474>.
- [31] P.T. Smith, A. Basu, A. Saha, A. Nelson, Chemical modification and printability of shear-thinning hydrogel inks for direct-write 3D printing, *Polymer (Guildf)*. 152 (2018) 42–50. <https://doi.org/10.1016/j.polymer.2018.01.070>.
- [32] N. Paxton, W. Smolan, T. Böck, F. Melchels, J. Groll, T. Jungst, Proposal to assess printability of bioinks for extrusion-based bioprinting and evaluation of rheological properties governing bioprintability, *Biofabrication*. 9 (2017) 044107. <https://doi.org/10.1088/1758-5090/aa8dd8>.
- [33] I. Díazñez, C. Gallegos, E. Brito-de la Fuente, I. Martínez, C. Valencia, M.C. Sánchez, M.J. Diaz, J.M. Franco, 3D printing in situ gelification of  $\kappa$ -carrageenan solutions: Effect of printing variables on the rheological response, *Food Hydrocoll.* 87 (2019) 311–330. <https://doi.org/10.1016/j.foodhyd.2018.08.010>.
- [34] A.C. Heidenreich, M. Pérez-Recalde, A. González Wuse, E. F. Hermida, Collagen and chitosan blends for 3D bioprinting: A rheological and printability approach, *Polym. Test.* 82 (2020) 106297. <https://doi.org/10.1016/j.polymertesting.2019.106297>.
- [35] A.D. Doyle, Generation of 3D Collagen Gels with Controlled Diverse Architectures, *Curr. Protoc. Cell Biol.* 72 (2016) 1–22. <https://doi.org/10.1002/cpcb.9>.
- [36] A.K. Mishra, J.P. Campanale, J.A. Mondo, V.J. Montell, Cell interactions in collective cell migration, *Development*. 146 (2019) dev172056. <https://doi.org/10.1242/dev.172056>.
- [37] D. Cordero Cervantes, C. Zurzolo, Peeling into tunneling nanotubes—The path forward, *EMBO J.* (2021) e105789. <https://doi.org/10.15252/embj.2020105789>.

## Graphical Abstract



## Highlights

- Highly controlled and reproducible 3D environment for cancer cell culture.
- Collagen/alginate/gelatine hydrogel as biomaterial-ink for cancer cell bioprinting.
- TNT-like structures assembly in 3D bioprinted cancer cells.

Journal Pre-proof

## Author Statement

### **Three-dimensional bioprinted cancer models: a powerful platform for investigating tunnelling nanotube-like cell structures in complex microenvironments.**

Helena Herrada-Manchón, Lucía Celada, David Rodríguez-González, M. Alejandro Fernández, Enrique Aguilar and María-Dolores Chiara.

#### **CRedit author statement**

**Helena Herrada:** Conceptualization, Methodology, Formal analysis, Investigation, Visualization, Writing- Reviewing and Editing **Lucia Celada:** Methodology, Formal analysis, Investigation, Visualization. **David Rodriguez:** Investigation; Methodology. **M Alejandro:** Conceptualization, Project administration, Supervision. **Enrique Aguilar:** Supervision, Writing- Reviewing and Editing. **María-Dolores Chiara:** Conceptualization, Supervision, Project administration, Funding acquisition, Writing- Reviewing and Editing

**Declaration of interests**

The authors declare that they have no known competing financial interests or personal relationships that could have appeared to influence the work reported in this paper.

The authors declare the following financial interests/personal relationships which may be considered as potential competing interests:

Journal Pre-proof